Bimolecular Kinetics at Low Temperatures Using FTIR Matrix Isolation Spectroscopy: Some Caveats. Thermokinetic Parameters for the Reaction of Fulvenones with Pyridine in Pyridine Matrixes

John Andraos*

The University of Queensland, Department of Chemistry, Brisbane, Queensland, 4072 Australia

Received: October 12, 1999; In Final Form: November 30, 1999

The bimolecular kinetics of addition of pyridine to fulvenone (**1**), benzofulvenone (**2**), and dibenzofulvenone (**3**) in pyridine matrixes at 15 to 70 K have been investigated by FTIR matrix isolation spectroscopy. A detailed kinetic analysis reveals a one-to-one correspondence between the disappearance of ketenes and the appearance of the corresponding ketene−pyridine zwitterions ("ketene ylides") formed upon nucleophilic addition. Perturbed second-order kinetics according to the Kohlrausch model were found to describe the data adequately, whereas pseudo-first-order and strict second-order kinetics did not. These results indicate that the bimolecular reaction examined takes place in a heterogeneous medium where distributions of second-order rate constants are obtained. The heterogeneity index, α, obtained from the model varies from 0.35 to 0.56. These findings are consistent with the matrix model proposed by Raff in which the structure of the pyridine matrix is composed of inhomogeneous fast sites where the magnitude of the true reaction rate for chemical reaction exceeds the diffusion rates of both ketene and pyridine molecules. Arrhenius and Eyring thermokinetic parameters obtained from these data reveal that the barrier for reaction under these conditions is very small (less than 1 kcal mol^{-1}) with a very large negative entropy of activation (ca. − 80 cal K^{-1} mol^{-1}). When compared with analogous solution phase kinetic results from laser flash photolysis experiments, it is concluded that the kinetics observed at these low-temperature conditions are largely that of matrix reorganization. This sets a lower limit for the rates and an upper limit for the activation parameters of the actual chemical reactions. Furthermore, identical magnitudes for E_A, $\Delta H^{\ddagger}$, and $\Delta S^{\ddagger}$ are found even when they are calculated from second-order rate constants based on the incorrect bimolecular model applicable to homogeneous media. It is suggested that the technique of dynamic matrix isolation spectroscopy is not adequate to obtain chemically meaningful activation parameters in bimolecular reactions. Caveats are also pointed out concerning the experimental interpretations of nonlinear Arrhenius plots obtained in cryogenic matrixes, implicit assumptions about the constancy of medium properties in the construction of Arrhenius and Eyring plots, and the calculation of thermokinetic parameters from data fits to linear forms of the Arrhenius and Eyring equations.

Introduction

Matrix isolation spectroscopy has proven to be a valuable technique for the characterization of short-lived intermediates at low temperatures. The majority of intermediates studied under these conditions have been radicals or carbenes examined by ESR, UV, and IR spectroscopy. Although the results of static experiments are abundant in the literature, kinetic investigations under these conditions are less frequently documented and are therefore the subject of considerable interest. Examples relevant to mechanistic organic chemists include decays of triplet carbenes in glassy or crystalline hosts[1] or in noble gas matrixes,[2] decays of triplet state aryl cations in microcrystalline powders and LiCl−water glasses,[3] decays of methyl radicals in crystalline matrixes of acetonitrile-d_3,[4] decays of triplet 1,3-cyclopentadiyl biradicals in cyclohexane matrixes,[5] and decays of triplet 1,3-cyclobutanediyl biradicals in glassy solvents.[6] Most of these studies probed unimolecular reactions of the given intermediates with the surrounding heterogeneous media.

The determination of associated thermokinetic parameters such as activation energies and entropies of activation in the above systems has been challenging mainly because kinetic analyses of decay traces do not follow simple pseudo-first-order rate laws applicable to homogeneous chemical systems. Instead, they are described as "stretched exponentials". By far, the most commonly used expression to treat such kinetic data is the Kohlrausch relaxation function[7] given by eq 1,

$$c = c_0 \exp\left[-\left(\frac{t}{\tau_0}\right)^{\alpha}\right] \tag{1}$$

where c is the time-dependent concentration of intermediate, c_0 is the initial concentration of intermediate, and τ_0 and α are constants ($0 < \alpha \leq 1$). This is analogous in form to the standard first-order rate law where the α parameter describes the degree of perturbation from a true first-order decay. Note that the normal equation with lifetime τ_0 is obtained when $\alpha = 1$. Another equation used by workers in the field which is identical in form to eq 1 is

$$c = c_0 \exp[-(kt)^{\beta}] \tag{2}$$

The connecting relations between eqs 1 and 2 are $\alpha = \beta$ and $k = \tau_0^{-1}$. Kinetic traces obeying either eq 1 or 2 are characterized

* Corresponding author. Current address: Department of Chemistry, York University, Toronto, ON M3J 1P3, Canada.

10.1021/jp993648a CCC: $19.00
Published on Web 01/25/2000

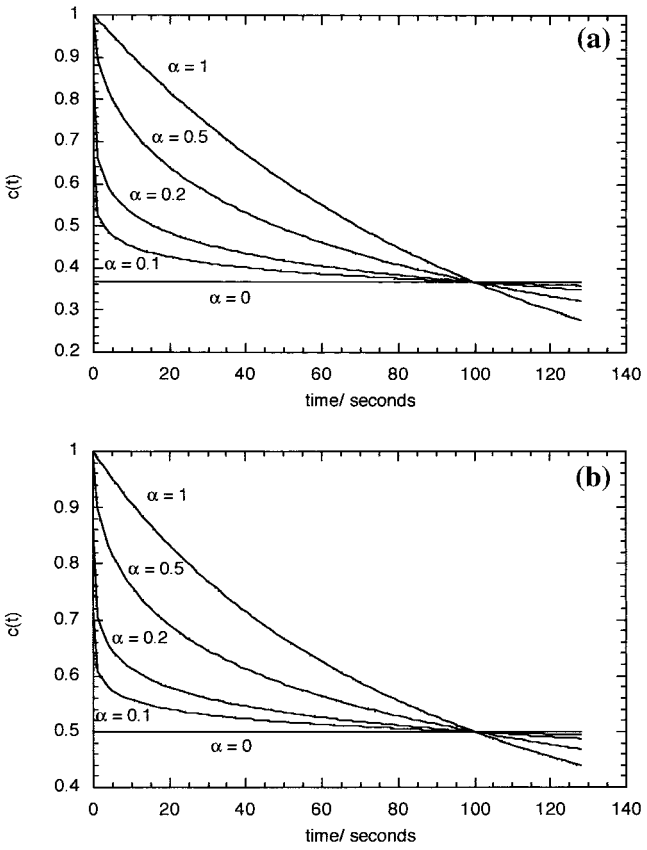

Figure 1. (a) Simulation of first-order perturbed decay trace according to eq 1 for various α values. (b) Simulation of second-order perturbed decay trace according to eq 4 for various α values. In each case, $c_0 = 1$ and $k_0 = 0.01$.

by two distinct regions: a very rapid decay occurring at short times and a very slow "stretched out" decay occurring over much longer times. These may be verified by examining the variation of the derivative or tangent line to the curve with time. As t approaches 0, the slope of the tangent line approaches infinity; and as t approaches infinity, the slope of the tangent line approaches 0. In contrast, a similar analysis of the time-dependent behavior of the derivative function for the normal first-order decay expression results in a finite value of $-c_0/\tau_0$ for the slope at $t = 0$ and a much faster approach to a zero slope (reaction completion) as t approaches infinity. As noted from parts a and b of Figure 1, the smaller the magnitude of the heterogeneity index at constant k, the greater is the degree of steepness of the initial part of the kinetic trace and the longer it takes to approach reaction completion.

The perturbed pseudo-first-order relationship has been successfully used to describe the nonexponential decays of a variety of relaxation phenomena in amorphous and polycrystalline solids, polymer matrixes, and aqueous micellar solutions.[8] A specific variant of eq 1 with $\alpha = 0.5$ known as the root t law has also found extensive application.[9] Although it was first introduced as an empirical relationship, the Kohlrausch relaxation function has been verified using the continuous time random walk (CTRW) model[10] whose central result is that the rate constant coefficient, k, for a chemical reaction taking place in condensed media is time dependent and has the form

$$k(t) \approx t^{\alpha-1} \tag{3}$$

where $0 < \alpha \leq 1$. Physical interpretations of the obtained rate constant and α parameters have been the subject of intense discussion (vide infra).[11]

SCHEME 1

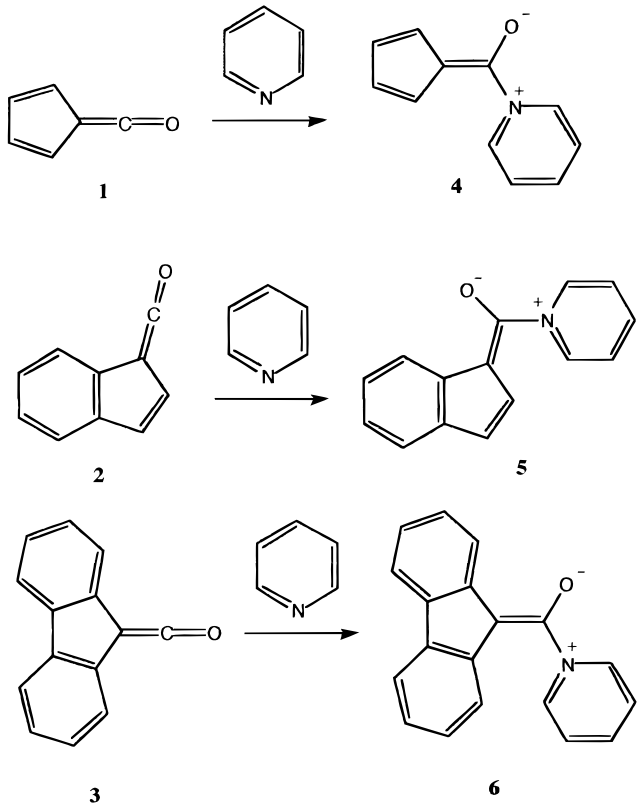

On the other hand, kinetic studies of bimolecular reactions in heterogeneous media are few in number and are mainly dominated by the work of Plonka. The best examples are geminate radical or ion recombination reactions in polymer matrixes,[12] low-temperature glasses,[13] or liquid cyclohexane;[14] recombination of carbon monoxide with myoglobin in frozen glycerol−water solutions;[15] and electron scavenging by alkyl halides in cyclohexane solutions.[16] In these studies, Plonka used an extended Kohlrausch relation given by eq 4,

$$c = \frac{c_0}{1 + c_0(kt)^{\alpha}} \tag{4}$$

applicable to equal concentration second-order kinetics to treat the "stretched hyperbolic" kinetic data. From these results time-dependent activation energies as well as rate constant and activation energy distributions were obtained. Building on these investigations, we sought to test the Plonka analysis on a chemical system which has been well studied experimentally[17] and theoretically,[18] namely, the nucleophilic addition of amines to ketenes. In this paper, we extend our preliminary kinetics investigation on the bimolecular reaction of fulvenones **1**, **2**, and **3**, generated by photo-Wolff rearrangement from diazoketone precursors, with pyridine in pyridine matrixes to form the corresponding zwitterion adducts (Scheme 1).[19] A detailed quantitative kinetic analysis is presented and thermokinetic parameters for the reactions are obtained. These results are discussed in light of the physical interpretations of rate constant, k, heterogeneity index, α, and thermokinetic parameters and the structure of the matrix. In addition, comparisons are made with solution phase kinetic studies done on the same systems by laser flash photolysis in aqueous[20] and acetonitrile solutions[21] at room temperature. Caveats related to using the technique of matrix isolation spectroscopy at low temperatures as a tool for performing kinetics experiments are also presented.

Experimental Section

Apparatus. An APD Cryogenics cryostat, CSW-204SL-6.5K, equipped with KBr windows and a Lakeshore model 330-44 temperature controller were used. In a typical bimolecular reaction, the diazoketone precursor was co-condensed at 6.5−8.0 K with a large excess of pyridine vapor (at least 100:1) and subsequently converted to the corresponding ketene by irradiation at the lowest possible temperature. The conditions for deposition of the diazoketones at 6.5 K and 10^{-5} Torr were as follows: (1) 1-diazobenzene-2-oxide, sublimed at −5 to −10 °C for 5 min; (2) 2-diazonaphthalene-1-oxide, sublimed at 60−65 °C for 7 min; (3) 9-diazophenanthrene-10-oxide, sublimed at 55−60 °C for 5 min. For most experiments, the following setup was employed. To the cold head assembly was attached a V-shaped glass manifold having two inlet ports to allow simultaneous entry of diazoketone and pyridine vapors toward the cold window. The diazoketones were sublimed from cylindrical glass tubes equipped with Teflon screw valves that allowed control of the vapor flow. These sample tubes were immersed in heating or cooling baths and allowed to equilibrate for a period of 15 min prior to deposition. Pyridine vapor was introduced from a reservoir containing spectroscopic grade pyridine liquid (99%) that was previously distilled over potassium hydroxide and subjected to three freeze−pump−thaw cycles. The flow of pyridine vapor through an evacuated copper line was controlled by means of a needle valve (Balzers). All glass attachments were made with KF10 connectors and associated Teflon clamps. Because of the reduced volatility of 9-diazophenanthrene-10-oxide compared with the other two diazoketones under these conditions, the sample tube assembly was not used. Instead, a 5−10 mg sample of the compound was placed directly inside a glass sublimation tube which was wrapped with heating wire, and this sample was then sublimed in a stream of pyridine vapor.

Photolysis. Photolyses were carried out using a low-pressure Hg lamp (75 W, 254 nm maximum output operated at 100 mA; Gräntzel, Karlsruhe, Germany) positioned about 5 cm from the quartz window aperture of the cold head assembly. Photolysis periods were as follows: (1) 1-diazobenzene-2-oxide, 15 min; (2) 2-diazonaphthalene-1-oxide, 30 min; (3) 9-diazophenanthrene-10-oxide, 70 min for complete conversion to the corresponding ketenes.

Acquisition of Kinetic Data. Infrared spectra were recorded on a Perkin-Elmer System 2000 FTIR spectrometer using a liquid nitrogen cooled MCT (HgCdTe) detector. A time-resolved IR (TRIR) subprogram to the main IRDM (IR Data Manager) software supplied by Perkin-Elmer was used for performing kinetic experiments. In a typical run, a background spectrum was first recorded (two scans) at a given temperature, usually 10 K. Spectral ranges corresponding to the ketene (2180−2060 cm^{-1}) and zwitterion (1710−1640 cm^{-1}) intermediates were selected. The cold window was then allowed to warm rapidly to a new temperature 5 degrees higher within 5−10 s. Immediately after stabilization at this temperature, difference IR spectra in each spectral window were recorded (two scans each) at intervals of 0.6 s for a period of 5−8 min. On the basis of the degree of depletion of ketene absorption bands this represented a reaction conversion of about 50%. For rapid scanning, the biseparational mode was selected in which scanning from 4000 to 450 cm^{-1} and from 450 to 4000 cm^{-1} was possible. There was no delay between the moment of manually triggering the spectrometer and the start of data acquisition. Graphs representing the variation of integrated difference absorption peak areas against time were simultaneously recorded for the ketene and zwitterion spectral ranges. These kinetic traces consisting of at least 500 data points each were then fit to various kinetic expressions using SigmaPlot (Jandel Scientific) or KaleidaGraph (Synergy Software) statistical programs. When no further spectral changes were observed in a given run the rapid warm-up cycle was repeated at the next higher temperature. At each new temperature a new background spectrum was recorded. The maximum temperature reached in the warm-up cycles was 70 K, as heating above this temperature resulted in a significant increase in signal noise and hence kinetic data obtained were unreliable. The accuracies of the recorded temperatures upon warm-up are ±3 K from 6.5 to 30 K and ±1 K for temperatures above 30 K. Since it was difficult experimentally to maintain constant temperatures after fast warm-up increments of 5 K at the highest heating rate in the temperature range 6.5−30 K, a medium heating rate was selected to prevent overshooting of the temperature and thus causing considerable structural changes in the matrix that would have resulted in a sudden rapid consumption of ketene. For temperatures above 30 K, this problem did not occur, and a high heating rate was used. Because of these temperature control problems and the need to have as best as possible reproducible starting matrixes for each run in a set, obtaining reproducible kinetic data by these methods proved to be quite difficult. Experiments were therefore performed at least three times for each diazoketone examined. Only the best pairwise sets of data for ketene depletion and zwitterion production for each compound were selected for Arrhenius and Eyring analyses.

TABLE 1: Maxima of the Monitored Infrared Absorption Bands for Fulvenones and Fulvenone−Pyridine Zwitterions in Pyridine Matrixes

ketenes	ω/cm^{-1}	zwitterions	ω/cm^{-1}
1	2126	**4**	1683
2	2128, 2117.5	**5**	1675
3	2115	**6**	1653

Materials. 1-Diazobenzene-2-oxide, 2-diazonaphthalene-1-oxide, and 9-diazophenanthrene-10-oxide were synthesized according to procedures reported in our earlier work.[19]

Results and Discussion

1. Kinetic Data. *Acquisition.* Kinetic data were obtained by recording integrated FTIR difference spectra as a function of time as described in the Experimental Section. Table 1 summarizes the maxima of the infrared absorption bands for fulvenones **1**, **2**, and **3** and the corresponding fulvenone−pyridine zwitterions in pyridine matrixes. The spectral characteristics and their time-dependent behavior were similar to those shown in our earlier work.[19] Ketene bands appeared strong and intense, whereas zwitterion bands appeared weak and broad. In the difference spectra representation, the change in the intensity of the ketene band increases in the negative direction, consistent with the increase in consumption of the fulvenone as the reaction proceeds; whereas, the change in intensity of the zwitterion band increases in the positive direction consistent with the increase in production of the adduct as the reaction proceeds.

In the analysis of the kinetic data, we first assume that the selected absorption bands are Gaussian in shape and are unique absorptions due to the individual chemical species with no interfering absorptions from other species. Therefore, peak intensities (absorbance, A) scale linearly with peak areas

(integrated absorbance, I).[22] In the co-deposition of diazoketone vapor with excess pyridine vapor we further assume an initial matrix at the lowest temperature with each guest diazoketone molecule surrounded by several host pyridine molecules so that the isolation criterion is met. Experimentally this criterion is fulfilled when recorded spectra are observed to have sharp absorption lines. The implication is that, after complete photolysis of the diazoketone photoprecursors at the lowest possible temperature, the isolation criterion is again satisfied so that the resultant matrix is composed of newly formed guest ketene molecules being surrounded by host pyridine molecules after photo-Wolff rearrangement has occurred. The ratio of host pyridine molecules to guest ketene molecules is at least 100:1 since the percent change in intensity of the strongest pyridine absorption band at 1438 cm^{-1} during the warm-up sequence is observed to be less than 1%. Hence, the overall consumption of pyridine during the reaction is small, whereas the consumption of ketene is readily observed as the intensity of the absorption band in the 2100 cm^{-1} region diminishes dramatically during the course of the reaction. It is obvious that the task of obtaining reproducible deposition and photolyzed matrixes is critical to the outcome of the kinetics experiment.

The elementary bimolecular reaction examined in this investigation, the addition of pyridine to ketene, is represented by the general chemical equation

$$K + P \rightarrow Z$$

where K, P, and Z represent ketene, pyridine, and zwitterion, respectively. The rate law for this reaction in terms of time-dependent concentrations is given by

$$\frac{d[Z]}{dt} = -\frac{d[K]}{dt} = -\frac{d[P]}{dt} = k[K][P] \qquad (5)$$

where k is the second-order rate constant for the nucleophilic addition.

Raff has proposed a general N-zone matrix model[23] and presented a number of limiting cases for a bimolecular reaction of the type given in eq 5. In his description, a matrix is composed of zones and each zone in turn is composed of sites. If a matrix is composed of one zone, then it is called homogeneous; if it is composed of several zones then it is called inhomogeneous. The property of matrix homogeneity is then applied to zones not sites so that the degree of homogeneity is related inversely to the number of zones. Hence, all sites within a given zone have the same degree of homogeneity. Sites may be classified as slow or fast depending on the relative magnitudes of the rate constant for bimolecular reaction to produce product and the diffusion coefficients of reactants describing the diffusion of reactant molecules from one site to the next or from one zone to the next. From our experimental results, we can infer (vide infra) that immediately after an incremental warm-up of the matrix to a higher temperature, we are observing reaction of the ketenes with the immediate nearest neighbor pyridine molecules and very little from bulk pyridine. Hence, the "effective" concentrations of ketene and pyridine leading to reaction are essentially equal. Using Raff's terminology, the present pyridine matrix is classified as inhomogeneous (multizonal) with fast sites so that the rate of reaction to produce zwitterion is faster than either the rate of diffusion of reactants within a given zone (intrazonal diffusion or, equivalently, diffusion between sites in the same zone) or that between zones (interzonal diffusion or, equivalently, between a site in one zone and another site in another zone).

The expressions for the time-dependent disappearance of ketene and the appearance of zwitterion derived from eq 5 are given by

$$[K] = \frac{[K]_0 - [K]_\infty}{1 + k[K]_0 t} + [K]_\infty \qquad (6a)$$

and

$$[Z] = \frac{k[K]_0([K]_0 - [K]_\infty)t}{1 + k[K]_0 t} \qquad (6b)$$

where $[K]_0$ and $[K]_\infty$ represent the ketene concentrations at the initial time of measurement and at very long times when reaction is allowed to reach completion, respectively. Note that the difference $[K]_0 - [K]_\infty$ corresponds to the maximum concentration of zwitterion produced in the reaction, $[Z]_\infty$. In the performed experiments, the first warm-up sequence begins at the lowest possible temperature, T_1 (10 K), with an initial concentration of ketene, $[K]_0$, and no zwitterion product present, $[Z]_0 = 0$. The matrix is then warmed to a higher temperature T_2, whereupon reaction is monitored for 5−8 minutes. At the end of this time period, τ, there remains in the matrix unreacted ketene, $[K]_\tau$, and the zwitterion product, $[Z]_\tau = [K]_0 - [K]_\tau$. In general, for any warm-up sequence, the corresponding pair of equations may be conveniently written as

$$[K] = \frac{[K]_{initial} - [K]_{final}}{1 + k[K]_{final} t} + [K]_{final} \qquad (7a)$$

and

$$[Z] = \frac{k[Z]_{initial}([Z]_{initial} - [Z]_{final})t}{1 + k[Z]_{initial} t} \qquad (7b)$$

where $[K]_{initial}$ and $[Z]_{initial}$ are taken to represent the initial concentrations of ketene and zwitterion present in the matrix at the start of a kinetic run where data are recorded immediately after warm-up to a higher temperature, and $[K]_{final}$ and $[K]_{final}$ are taken to represent the final concentrations of these species if the reaction was allowed to proceed to completion. Eqs 7a and 7b may be written in terms of peak absorbances (peak heights), A, or integrated peak absorbances (peak areas), I, which are the experimental observables, as outlined in Appendix A. Since difference spectra are recorded, the applicable equations for data fitting to true second-order behavior are eqs A8 and A9.

Data Fitting. Kinetic traces fit to expressions corresponding to strict second-order behavior yielded calculated lines that did not fit any of the collected data adequately. Following the graphical linearity test suggested by Raff,[23b] Figure 2 shows the result of a fit using a linearized transformation of eq A8 and its corresponding residual plot. It is clear that homogeneous-like behavior is not applicable to the present kinetic investigation in pyridine matrixes. From the Raff analysis, we may conclude that the matrix is not homogeneous; that is, it consists of more than one zone and therefore the kinetic behavior cannot be described by a single second-order expression. Hence, the Plonka treatment using a Kohlrausch analysis appropriate for equal concentration second-order kinetics was adopted using the expressions below:

$$-\Delta I_K = a - \frac{b}{1 + ct^\alpha} \qquad (8a)$$

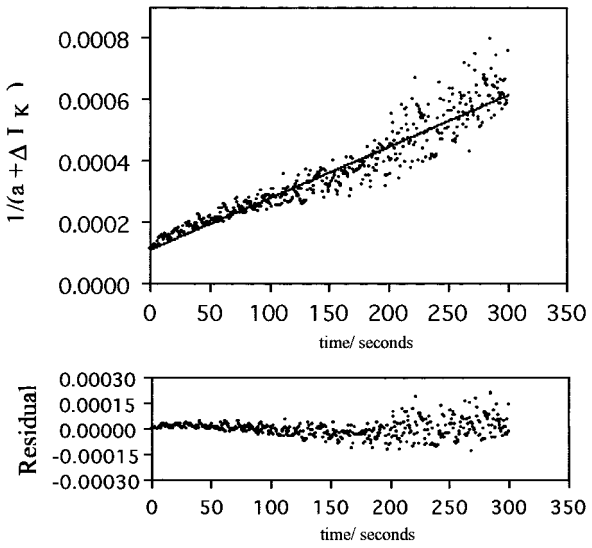

Figure 2. (top) Linearized transformation of observed kinetic trace corresponding to the difference ketene peak integrated absorbance, $-\Delta I_K$, as a function of time for the reaction of fulvenone **1** with pyridine in pyridine matrixes at 40 K. The calculated line is a fit according to the linearized form of the strict second-order model equation (A8): $k = 3.90 \times 10^{-6}$ M^{-1} s^{-1}, $\alpha = 1$. (bottom) Residual plot of data fit.

where $a = I_{K,b} - I_{K,final}$, $b = I_{K,1} - I_{K,final}$, and $c = I_{K,1}k'^{\alpha}$, and

$$\Delta I_Z = \frac{bt^{\alpha}}{1 + ct^{\alpha}} + a \qquad (8b)$$

where $a = I_{Z,1} - I_{Z,b}$, $b = k''^{\alpha} I_{Z,1}(I_{Z,final} - I_{Z,1})$, and $c = k''^{\alpha} I_{Z,1}$. These expressions represent perturbed second-order behavior applicable to inhomogeneous media. Nonlinear least-squares analysis of kinetic traces to these expressions yielded estimates of the rate constant and α parameters. The best kinetic data obtained for the three fulvenones are given in Tables S1−S3 of the Supporting Information and example kinetic plots for the consumption of fulvenone **1** and production of its zwitterion adduct at 40 K are shown in Figures 3 and 4. For comparison, results of data fits to the strict second-order model are also included in the tables. It should be noted that the shapes of the kinetic traces shown are consistent with the description of "stretched" kinetic curves given in the Introduction with respect to a fast component at short time scales and a rather slow component at longer time scales. In all cases, the kinetics of disappearance of ketene coincided with that of appearance of zwitterion ($k' = k''$). As expected, traces for zwitterion production were smaller in amplitude and noiser than those for ketene consumption owing to the weak and broad absorption bands of the zwitterions as discussed earlier. An important observation from these data is that in each data set the value of α is constant over the temperature range examined. Hence, for fulvenones **1**, **2**, and **3**, the pairwise mean values of α for ketene and zwitterion traces are 0.52 ± 0.03, 0.56 ± 0.03; 0.36 ± 0.05, 0.35 ± 0.06; and 0.42 ± 0.06, 0.37 ± 0.03, respectively. The constancy of α implies that the medium properties do not change over the temperature range examined and that the number of zones in the matrixes is the same; that is, the degree of inhomogeneity of the matrix medium is constant.

2. Physical Interpretation of Parameters. In standard homogeneous kinetics, reaction rates are constant since in such media it is assumed that the time scales for reaction are much longer than those of diffusion of reactants and environmental rearrangements of the medium itself. Rate constants are therefore constant and invariant with time. However, in heterogeneous media the time scales for diffusion of reactants and medium rearrangements are slowed and become competitive with the time scale for reaction. In condensed media, rate constants are no longer constant but depend on time as predicted by the CTRW model (see eq 3). Time-dependent rate constants are

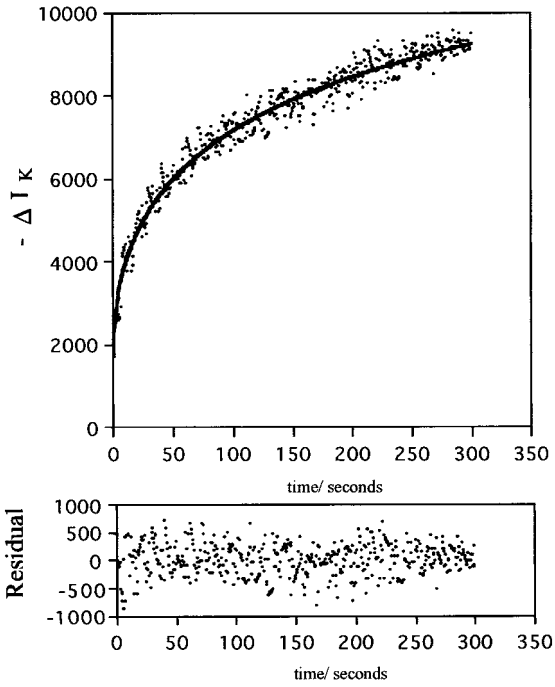

Figure 3. (top) Observed kinetic trace showing the dependence of the difference ketene peak integrated absorbance, $-\Delta I_K$, as a function of time for the reaction of fulvenone **1** with pyridine in pyridine matrixes at 40 K. The calculated line is a fit according to the perturbed second-order eq 8a: $k = 1.70 \times 10^{-6}$ M^{-1} s^{-1}, $\alpha = 0.48$. (bottom) Residual plot of data fit.

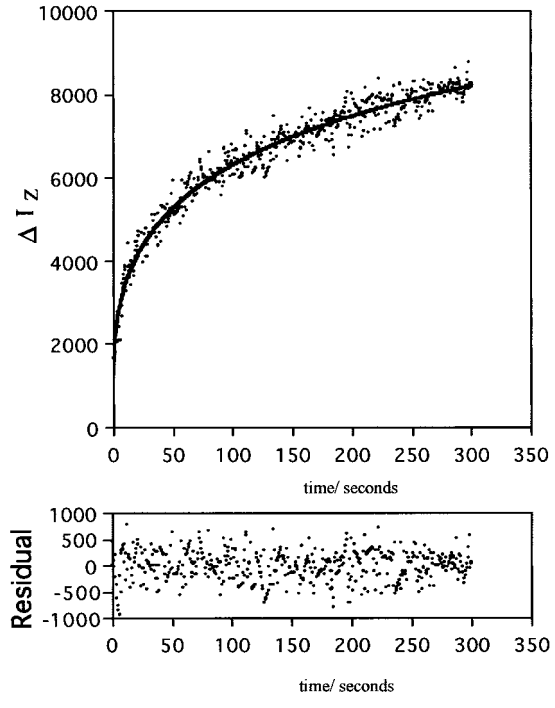

Figure 4. (top) Observed kinetic trace showing the dependence of the difference zwitterion peak absorbance, ΔI_Z, as a function time for the appearance of **4** formed from reaction of fulvenone **1** with pyridine in pyridine matrixes at 40 K. The calculated line is a fit according to the perturbed second-order eq 8b: $k = 2.00 \times 10^{-6}$ M^{-1} s^{-1}, $\alpha = 0.51$. (bottom) Residual plot of data fit.

manifested experimentally as decay curves exhibiting stretched exponential or hyperbolic characteristics. Consequently, there are two possible interpretations of time-dependent rate constants. The first is to treat rate constants obtained from stretched exponential decay curves as averages of distributions, not as single valued rate constants. The second is to link the time-dependent reactivity of species trapped in the medium with time-dependent energy barriers for reaction and for detrapping reactants. Matrix relaxation, therefore, is the physical energy associated with species leaving their "cages" or traps and entering new ones, and with the destruction of the vacated traps. The form of the time-dependent activation energy derived from eq 3 is given in Appendix B. Each of these interpretations can be used to rationalize the kinetic results of the present chemical system.

From standard statistical principles[24] distribution functions are intimately related to probability density functions. A density function of a given variable is more useful since fundamental properties of the distribution of that variable can be easily obtained from it such as the mean and variance. Also, density functions for other variables may be obtained from a parent density function of a given variable if the connecting relationships between the new and parent variables are known. The parameters k' and k'' obtained from eqs 8a and 8b represent average rate constant values. The α parameter, referred to as a dispersion parameter or heterogeneity index, is related to the width or the variance of the rate constant distribution. Hence, it is expected that as α approaches unity (homogeneous limit), the distribution width narrows and that as α approaches zero (completely heterogeneous limit), the distribution widens.

Furthermore, a distribution of rate constants may be interpreted as a superposition of discrete "homogeneous-like" rate constants or as a distribution of activation energies. In the first case, a stretched kinetic curve is analyzed as a sum of individual homogeneous kinetic curves. The result is a discrete distribution of rate constants rather than a continuous one. This is the basis of the exponential series method (ESM)[25] applied to first-order decay processes which results in discrete distributions of pseudo-first-order rate constants. Raff has proposed an equivalent hyperbolic series method[23] applicable to second-order processes in heterogeneous media where a stretched hyperbolic decay obeying eq 4 is written as

$$c = \frac{c_0}{1 + c_0(kt)^{\alpha}} = \sum_j \frac{c_{j,0}}{1 + c_{j,0}k_j t} \tag{9}$$

In the second case, a distribution of activation energies is obtainable using the Arrhenius relation once the parent distribution of rate constants is known. In this case, both distributions are continuous.

Plonka has stated[8a,11,15] that the "lifetime" density function corresponding to the second-order equal concentration model used here is given by

$$f(\tau) = \frac{\sin(\pi\alpha)}{\pi\tau} \frac{(\tau/\tau_0)^{\alpha}}{(\tau/\tau_0)^{2\alpha} + 2\cos(\pi\alpha)(\tau/\tau_0)^{\alpha} + 1} \tag{10}$$

where $0 < \alpha < 1$, $\tau = 1/c_0^{1/\alpha}k$, and $\tau_0 = 1/c_0^{1/\alpha}k_0$. The corresponding rate constant density function found from the method of transformations[24] is

$$f(k) = \frac{\sin(\pi\alpha)}{\pi k} \frac{(k_0/k)^{\alpha}}{(k_0/k)^{2\alpha} + 2\cos(\pi\alpha)(k_0/k)^{\alpha} + 1} \tag{11}$$

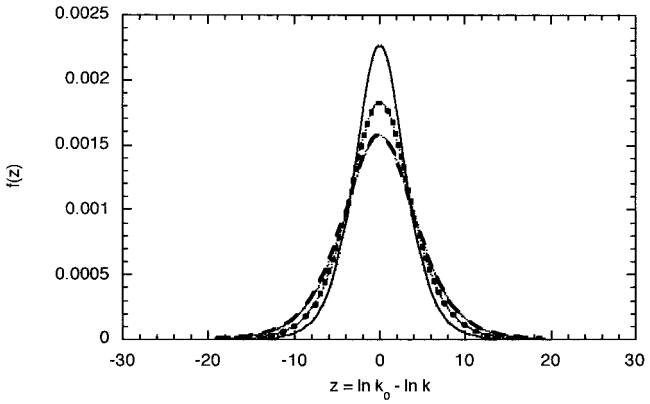

Figure 5. Probability density functions according to eq 12 for the disappearance of fulvenones in pyridine matrixes at 15−70 K: (a) fulvenone ($\alpha = 0.52$, —), (b) benzofulvenone ($\alpha = 0.36$, - - -), and (c) dibenzofulvenone ($\alpha = 0.42$, · · ·).

It is more convenient to derive the density function for the difference $\ln k_0 - \ln k$ since it is immediately related to the difference in activation energies through the Arrhenius equation. Hence, again by the method of transformations,

$$f(z) = \frac{\sin(\pi\alpha)}{\pi} \frac{\exp(z\alpha)}{\exp(2z\alpha) + 2\cos(\pi\alpha)\exp(z\alpha) + 1} \tag{12}$$

where $z = \ln(k_0/k) = \ln k_0 - \ln k$. It can be shown that the mean and variance of z are 0 and $(\pi^2/3)((1 - \alpha^2)/\alpha^2)$, respectively (see Appendix C). The variance is a measure of the distribution width. It is apparent then that as the degree of heterogeneity of the medium increases ($\alpha \rightarrow 0$), the distribution width increases ($\sigma_z^2 \rightarrow \infty$), whereas, as the degree of homogeneity increases ($\alpha \rightarrow 0$), the distribution width narrows ($\sigma_z^2 \rightarrow 0$). It can also be shown that if the rate constant is interpreted as a discrete random variable, then the average value k_0 is the geometric mean of the discrete set of rate constants describing the distribution (see Appendix C). This set of rate constants corresponds to the set of homogeneous-like kinetic traces used to describe the overall stretched trace (see eq 9). The corresponding distribution function for the density function in eq 12 is given by

$$F(z) = \int f(z)\,dz = \frac{\sin(\pi\alpha)}{\pi\alpha(B - A)} \ln\left[\frac{\exp(z\alpha) + A}{\exp(z\alpha) + B}\right] \tag{13}$$

where $A = \exp(\pm i\pi\alpha)$ and $B = \exp(\mp i\pi\alpha)$. Figure 5 shows the density functions according to eq 12 for the three fulvenones.

The characteristics of the density function given in eq 12 are identical to those for the density function for the difference *activation energy for detrapping reactants*[8a,11]

$$f(E - E_0) = \frac{\sin(\pi\alpha)}{\pi RT} \frac{\exp\epsilon}{\exp(2\epsilon) + 2\exp\epsilon\cos(\pi\alpha) + 1} \tag{14}$$

where $\epsilon = \alpha(E - E_o)/RT$, $\langle E - E_0\rangle = 0$, and $\sigma_{E-E_0}^2 = (\pi^2/3)\cdot(RT)^2((1 - \alpha^2)/\alpha^2)$. For comparison, the density function for the difference *activation energy for reaction* is given by[8a,11]

$$f(E - E_0) = \frac{\epsilon\exp\epsilon}{(E - E_0)[1 + \exp\epsilon]^2} \tag{15}$$

where $\epsilon = \alpha(E - E_0)/(1 - \alpha)RT$, $\langle E - E_0\rangle = 0$, and $\sigma_{E-E_0}^2 = (\pi^2/3)(RT)^2((1 - \alpha)/\alpha)^2$.

TABLE 2: Thermokinetic Parameters for the Reactions of Fulvenones with Pyridine in Pyridine Matrixes Analyzed According to a Perturbed Second-Order Model

fulvenone	A	ln A	E_A/ kcal mol^{-1}	$\Delta H^{\ddagger}$/kcal mol^{-1}	$\Delta S^{\ddagger}$/cal K^{-1} mol^{-1}
			Ketene Kinetic Data		
1	$(7.1 \pm 2.6) \times 10^{-4}$	-7.2 ± 0.4	0.5 ± 0.1	0.4 ± 0.1	-72 ± 1
2	$(5.4 \pm 6.3) \times 10^{-5}$	-9.8 ± 1.2	0.1 ± 0.1	0.1 ± 0.1	-76 ± 2
3	$(7.9 \pm 6.8) \times 10^{-5}$	-9.5 ± 1.0	0.3 ± 0.1	0.2 ± 0.1	-75 ± 2
			Zwitterion Kinetic Data		
1	$(6.1 \pm 4.9) \times 10^{-4}$	-7.4 ± 0.8	0.4 ± 0.1	0.3 ± 0.1	-72 ± 2
2	$(3.8 \pm 4.2) \times 10^{-5}$	-10.2 ± 1.1	0.1 ± 0.1	0.1 ± 0.1	-76 ± 2
3	$(7.8 \pm 8.8) \times 10^{-5}$	-9.5 ± 1.1	0.3 ± 0.1	0.2 ± 0.1	-75 ± 2
			Combined Ketene and Zwitterion Kinetic Data		
1	$(6.9 \pm 3.9) \times 10^{-4}$	-7.3 ± 0.6	0.5 ± 0.1	0.4 ± 0.1	-72 ± 1
2	$(4.5 \pm 3.3) \times 10^{-5}$	-10.0 ± 1.0	0.1 ± 0.1	0.1 ± 0.0	-76 ± 1
3	$(7.8 \pm 4.9) \times 10^{-5}$	-9.5 ± 0.6	0.3 ± 0.1	0.2 ± 0.1	-75 ± 1

TABLE 3: Thermokinetic Parameters for the Reactions of Fulvenones with Pyridine in Pyridine Matrixes: Combined Ketene and Zwitterion Kinetic Data Analyzed According to a Strict Second-Order Model (Eqs A8 and A9)

fulvenone	A	ln A	E_A/kcal mol^{-1}	$\Delta H^{\ddagger}$/kcal mol^{-1}	$\Delta S^{\ddagger}$/cal K^{-1}mol^{-1}
1	$(4.3 \pm 3.7) \times 10^{-4}$	-7.8 ± 1.0	0.4 ± 0.1	0.3 ± 0.1	-73 ± 2
2	$(2.0 \pm 0.7) \times 10^{-7}$	-15.4 ± 0.4	0.1 ± 0.0	0.0 ± 0.0	-87 ± 1
3	$(1.2 \pm 0.5) \times 10^{-5}$	-11.3 ± 0.4	0.4 ± 0.0	0.3 ± 0.0	-79 ± 3

3. Thermokinetic Parameters and Matrix Structure. Since the calculated rate constants from the Kohlrausch model are actually average values as already noted, Arrhenius and Eyring treatments using these data result in estimates of the average values of the respective thermokinetic quantities. Hence, from the calculated average rate constants in Tables S1−S3 of the Supporting Information, estimates of the average activation energy, E_a, average enthalpy of activation, $\Delta H^{\ddagger}$, and average entropy of activation, $\Delta S^{\ddagger}$, for the bimolecular reaction may be made. As prescribed by others,[26] best estimates of these thermokinetic parameters were obtained by nonlinear least-squares analysis of the rate constant−temperature data according to equations of the form

$$k = m_1 \exp\left[-\frac{m_2}{T}\right] \tag{16}$$

where $m_1 = A$ and $m_2 = E_a/R$ and

$$k = m_1 T \exp\left[-\frac{m_2}{T}\right] \tag{17}$$

where $m_1 = k_B/h \exp[-\Delta S^{\ddagger}/R]$ and $m_2 = \Delta H^{\ddagger}/R$ rather than by linear least-squares analysis according to standard linearized forms of eqs 16 and 17. Table 2 summarizes the results using rate constants calculated from the perturbed second-order model, and Table 3 summarizes those calculated from the strict second-order model. An example Arrhenius plot for the reaction of fulvenone **1** with pyridine is also given in Figure 6. It is readily apparent that both models essentially give identical results, although it was already shown that the strict second-order model does not fit the kinetic data adequately.

From these data, one can conclude that the barrier for reaction is small and the entropy of activation is large and negative. Further support of the observed small barrier for reaction comes from recent theoretical calculations[18b] done on the parent fulvenone−pyridine system at 0 K which show that the activation barrier for this reaction is less than 3 kcal mol^{-1} (B3LYP/6-31G*). In addition, the probability densities shown in Figure 5 for $z = \ln k_0 - \ln k$ are also those for the detrapping activation energy difference, $E_0 - E$, where E_0 is the average activation energy corresponding to the average rate constant k_0 (see eqs 12 and 14). The implication from these density

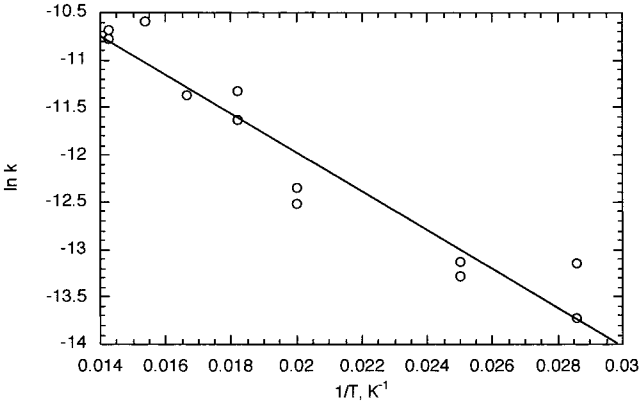

Figure 6. Arrhenius plot for the reaction of fulvenone **1** with pyridine in pyridine matrixes between 35 and 70 K using combined rate constant data for the disappearance of ketene and appearance of zwitterion. Rate constants were calculated using the perturbed second-order model equations 8a and 8b. The line drawn is constructed using the calculated activation energy, $E_A = 0.5 \pm 0.1$ kcal mol^{-1}, and Arrhenius pre-exponential factor, $A = (6.91 \pm 3.92) \times 10^{-4}$, obtained from a nonlinear least-squares fit according to the exponential form of the Arrhenius equation (eq 16).

functions is that the measured rate constants are composite; that is, they do not entirely represent *reaction* rate constants but involve significant contributions from diffusional processes. This and the highly ordered medium as indicated by a large negative $\Delta S^{\ddagger}$ suggest that the thermokinetic parameters obtained give information about matrix reorganization and diffusion of reactants rather than about the chemical reaction itself. Recalling Raff's terminology, the pyridine matrix is inhomogeneous and is composed of fast sites where the rate of chemical reaction exceeds all interzonal and intrazonal diffusion coefficients. At a given temperature there is a distribution of reactive sites in the matrix. Each of these reactive sites is characterized by a distribution of orientations of pyridine molecules surrounding the isolated ketene molecule; only those that are favorably oriented with the nitrogen atom in close proximity and in plane to the C_α carbon atom of the ketene will result in reaction. Once these reactive sites are depleted reaction stops and no further consumption of ketene is observed. When the matrix is warmed to a higher temperature, this causes a redistribution of both pyridine and ketene molecules through intrazonal diffusion so that new reactive sites are created. Reaction once again occurs

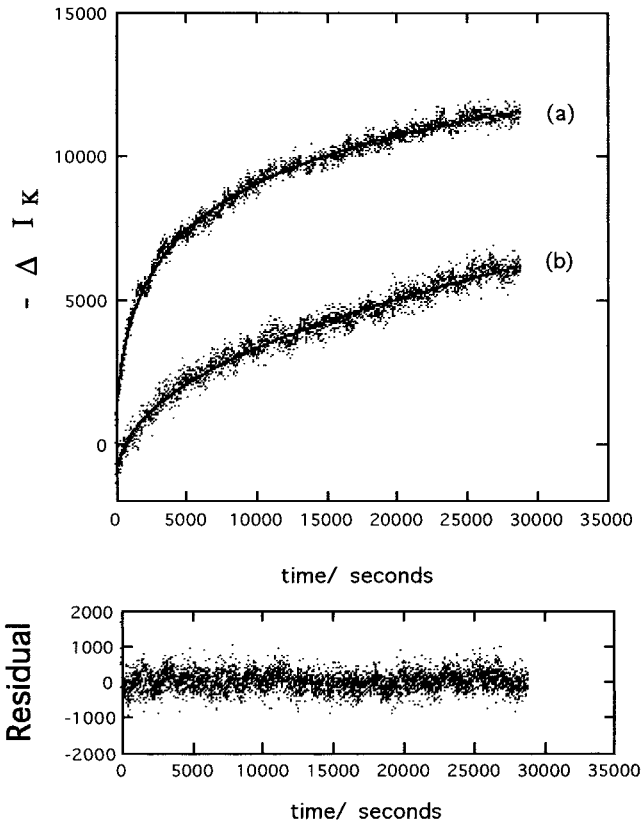

Figure 7. (top) Observed kinetic trace showing the dependence of the difference ketene peak integrated absorbance, $-\Delta I_K$, as a function of time for the reaction of dibenzofulvenone **3** with pyridine in pyridine matrixes after a 30 K → 40 K → 30 K warmup−cooldown cycle, (a) $k = 4.09 \times 10^{-7}$ M^{-1} s^{-1}, $\alpha = 0.51$. For comparison the corresponding observed kinetic trace for reaction at 30 K prior to the warmup−cooldown cycle is also shown, (b) $k = 7.89$ X 10^{-7} M^{-1} s^{-1}, $\alpha = 0.41$. (bottom) Residual plot of data fits.

until all of these new reactive sites have been exhausted. A sequence of warm-up cycles as done in these experiments results in the familiar "stepped" kinetics that are characteristic of kinetics observed in cryogenic media.

Further evidence of matrix reorganization and regeneration of new reactive sites was provided by a fast warm-up−cool-down cycle experiment, suggested by Wentrup, in the case of dibenzofulvenone **3**. When no further reaction was observed at 30 K, the matrix was quickly warmed to 40 K and then cooled back down to 30 K. Warm-up was carried out at the highest heating rate until 40 K was reached, and cooling was carried out by immediately switching off the heater on the temperature controller until the temperature fell just below 30 K. The entire cycle time was about 20 s. Immediately after the temperature reached 30 K, kinetic data were recorded as before for a period of 5 min. Figure 7 shows the resulting kinetic trace for the consumption of dibenzofulveneone after such a warm-up−cool-down cycle compared with the one obtained at 30 K before this cycle was carried out. As expected, the amplitude of the kinetic trace is smaller after this cycle than before since most of the reactive sites had already been depleted during the first reaction at 30 K. As a consequence of this, there are fewer new regenerated reactive sites that again could lead to reaction at 30 K. The process cannot however be repeated indefinitely since the number of sites containing ketene is finite to begin with and the turnover rate of unreactive sites to reactive ones is rapid.

The thermokinetic data obtained in these experiments may be compared with those from solution phase experiments done on analogous ketene structures. The hydration of ketene itself in water occurs with a modest barrier of $\Delta H^{\ddagger} = 10.3$ kcal mol^{-1} and $\Delta S^{\ddagger} = -16$ cal K^{-1} mol^{-1},[27a] whereas the hydration of sterically hindered ketenes occurs with $\Delta H^{\ddagger} = 4-7$ kcal mol^{-1} and $\Delta S^{\ddagger} \approx -50$ cal K^{-1} mol^{-1}.[27b] The reaction of para substituted phenylmethylketenes with various para substituted 1-phenylethanols in toluene solution occurred with $\Delta H^{\ddagger} = -0.9$ to 0.3 kcal mol^{-1} and $\Delta S^{\ddagger} = -71$ to -68 cal K^{-1} mol^{-1}.[27c] In the last case, a mechanism involving the intermediacy of an analogous zwitterion adduct between the alcohol and the ketene was invoked to explain the apparent highly ordered rate-limiting transition state leading to ester products.

4. Caveats Concerning Arrhenius Plots at Low Temperatures. Although not often stated, an inherent assumption in the construction of linear Arrhenius and Eyring plots is that the properties of the medium, specifically its structure, are constant over the temperature range examined. This is true for linear plots obtained for both homogeneous and heterogeneous media. If the heterogeneity index, α, is regarded as a property measurement of the medium, then a constant α value may be associated with linear Arrhenius plots. Specifically, in these experiments, observed constant α values suggest that the number of zones in the pyridine matrix is not changing over the temperature range examined. The resultant Arrhenius and Eyring plots (see Figure 6) are found to be linear between 20 and 70 K albeit the scatter in the data is largely due to the difficulty in maintaining adequate temperature control as the fast warmup cycles are performed. This is particularly true for temperatures in the region less than 30 K (see Experimental Section). Eventually, however, as the temperature continues to increase beyond 70 K, it is expected that the number of zones should decrease and that the matrix becomes more homogeneous ($\alpha \rightarrow 1$); that is, it approaches a single zone matrix structure. At this limit, true second-order kinetic behavior would be observed. Reduction of matrix zones at elevated temperatures would thus be associated with nonlinear Arrhenius behavior. An observed nonlinear Arrhenius plot may then be subdivided into linear segments each associated with a specific α value. Again, in these experiments the increase in opacity of the matrix and in evaporation of pyridine as the temperature was increased precluded observing nonlinear Arrhenius behavior. Overall, the region of linearity observed is small and our experimental limitations below and above the temperature window 20−70 K do not allow us to observe with confidence nonlinear Arrhenius behavior. However, the eventual occurrence of nonlinear behavior makes sense given the expectation of a gradual change in medium structure toward complete homogeneity at elevated temperatures. Further support for this is found when estimates are made of second-order rate constants at ambient temperatures using the thermokinetic parameters obtained in Table 2 and then are compared with known solution phase kinetic determinations. Laser flash photolysis experiments in acetonitrile solution of fulvenones **2** and **3** reacting with pyridine yield second-order quenching rate constants of 2.72×10^8 and 1.31×10^7 M^{-1} s^{-1}, respectively, at room temperature.[21] Results from extrapolations of thermokinetic data obtained here on these systems yield rate constants that are 13 orders of magnitude too slow. From determinations of appreciable energy barriers in analogous ketene bimolecular reactions (see above) it is clear that Arrhenius plots near room temperature are steeper than those at cryogenic temperatures. Hence, it is certain that an Arrhenius plot covering a much wider temperature range from 20 K ($\alpha = 0.35-0.56$) to 300 K ($\alpha = 1$) should be nonlinear and is consistent with the vastly different medium properties over this range.

Nonlinear Arrhenius plots in the cryogenic temperature domain have been observed before.[1,2] In most cases, the chemical systems studied were unimolecular transformations involving hydrogen atom transfers and the observed nonlinearity was attributed to quantum mechanical tunneling. It is likely that these conclusions are probably correct since unimolecular transformations are not governed by diffusional processes as much as bimolecular reactions. However, the results of experiments done in this work show that one must be careful in experimentally controlling the temperatures in this regime before concluding with confidence that nonlinear behavior is indeed occurring. This is especially true if kinetic data are collected using the fast warmup cycle scheme described here.

Another point of concern is in the evaluation of stretched exponential kinetic traces by the Kohlraush model. It should be emphasized that in the data fitting according to eqs 1 and 2 for first-order processes or to eqs 4, 8a, and 8b for second-order processes, the α parameter should not be artifically held fixed at some value between 0 and 1. Fixing the α value presupposes uniformity in the medium structure over the temperature range. This translates into an enforced linearity in the Arrhenius plot. Rather, the heterogeneity index should be allowed to float as a disposable parameter so that uniformity in the medium structure may be proven or disproven experimentally as done here.

Conclusions

FTIR spectroscopy has clearly shown that the reaction of ketenes with amines proceeds through a zwitterion adduct. Under cryogenic conditions, the bimolecular reaction follows perturbed equal concentration second-order kinetics according to the Kohlrausch model with small energy barriers and large negative entropies of activation. The thermokinetic parameters obtained in these experiments cannot be used to infer information about the corresponding solution phase parameters.

This work has highlighted a number of important experimental points concerning performing and interpreting thermokinetic data obtained in cryogenic matrixes.

(1) Dynamic matrix isolation spectroscopy appears not to be as useful a technique for obtaining chemically relevant thermokinetic parameters for bimolecular reactions as in the case of unimolecular reactions. Results from these experiments show that bimolecular reactions under these conditions are mainly governed by medium dynamics and diffusion.

(2) The Plonka analysis using the Kohlraush relaxation function and the interpretation of kinetics in condensed media in terms of distributions of rate constants and activation energies is consistent with Raff's *N*-zone matrix model whose kinetic analysis is also interpreted in terms of distributions of rate constants via exponential and hyperbolic series methods.

(3) Data fitting of kinetic traces collected at different temperatures according to the Kohlrausch model must be done without fixing the heterogeneity index, α. Furthermore, it is imperative to collect sufficient data points at short enough time scales in order to obtain reliable estimates of α since this parameter greatly influences the shape of kinetic traces obeying the Kohlrausch model in this time domain.

(4) Curvature in Arrhenius plots must be interpreted with care under cryogenic conditions, as the lack of temperature control may result in artifacts and incorrect conclusions drawn.

(5) Linear Arrhenius plots over a temperature range are associated with constant α values which in turn are associated with uniform medium structures over that temperature range. From the Raff *N*-zone matrix model, equal α's mean that the number of zones is the same. In addition, constant α values are associated with constant rate constant distribution widths.

(6) Nonlinear Arrhenius plots may be interpreted as a superposition of several linear Arrhenius plots where each linear region is associated with its own α value and hence its own medium structure.

Acknowledgment. This work was supported by the Australian Research Council. The author thanks the University of Queensland for a University of Queensland Post-doctoral Fellowship and a Junior Researcher Award, Mr. Greg Rees of the departmental mechanical workshop for assistance with computer software, Dr. G. G. -H. Qiao for assistance in preliminary experiments, and Prof. Yuri Berlin for clarification of the proof of eq 10. Also, Prof. Curt Wentrup is acknowledged for providing use of cyrostat equipment and FTIR spectrometers in his laboratory and for bringing references 10a and 23a to the author's attention.

Supporting Information Available: Tables S1, S2, and S3 giving kinetic data for the reactions of fulvenones with pyridine in pyridine matrixes for strict and perturbed second-order models; Tables S4a and S4b giving thermokinetic parameters for ketene depletion and zwitterion formation calculated using kinetic data obtained from a strict second-order model; and a complete proof of eq 10. This material is available free of charge via the Internet at http://pubs.acs.org.

Appendix A

Derivation of Time-Dependent Difference Peak Areas. Peak absorbances are related to concentrations through the Beer−Lambert relationship given by eq A1 with respect to the ketene species

$$A_K = \epsilon_K[K]l \tag{A1}$$

where ϵ_K and l are the molar absorption coefficient and path length, respectively. From our earlier assumption that the infrared absorption line shapes are Gaussian functions, a similar expression can be written down relating peak areas to concentrations as shown in eq A2 with respect to the ketene species

$$I_K = A_K\sigma\sqrt{\pi} = \epsilon_K l\sigma\sqrt{\pi}[K] \tag{A2}$$

Rewriting eqs 2b and 3b in terms of absorbance, A, or integrated absorbance, I, leads to identical forms except that the rate constant factor will include additional constants related to A and I as appropriate. In terms of absorbance, the analogous expressions for the ketene (K) and zwitterion (Z) are

$$A_K = \frac{A_{K,initial} - A_{K,final}}{1 + k'tA_{K,initial}} + A_{K,final} \tag{A3}$$

and

$$A_Z = \frac{k''tA_{Z,initial}(A_{Z,final} - A_{Z,initial})}{1 + k''tA_{Z,initial}} + A_{Z,initial} \tag{A4}$$

where $k' = k/\epsilon_k l$ and $k'' = k/\epsilon_z l$. In terms of integrated absorbance, the analogous expressions for the ketene and zwitterion are

$$I_K = \frac{I_{K,initial} - I_{K,final}}{1 + k'tI_{K,initial}} + I_{K,final} \tag{A5}$$

and

$$I_Z = \frac{k''tI_{Z,initial}(I_{Z,final} - I_{Z,initial})}{1 + k''tI_{Z,initial}} + I_{Z,initial} \qquad (A6)$$

where $k' = k/\epsilon_\kappa l\sigma\sqrt{\pi}$ and $k'' = k/\epsilon_\kappa l\sigma\sqrt{\pi}$.

In the time-resolved acquisition program, difference spectra were recorded at a temperature T_2 at regular time intervals using the spectrum recorded at the lower temperature T_1 as a background (see Experimental Section). Note that the ketene bands appear as negative peaks and the zwitterion bands as positive peaks in the difference spectra. Since the ketene is being consumed as it reacts with pyridine, the ketene absorption band is obviously decreasing in intensity and in peak area. In terms of peak areas, the *difference* peak areas for the ketene absorption are given by

$$I_{K,1} - I_{K,b}, I_{K,2} - I_{K,b}, I_{K,3} - I_{K,b}, ..., I_{K,n} - I_{K,b}$$

for $t = 0, t_1, t_2, ..., t_n$, where $I_{K,b}$ is the peak area recorded as the background spectrum at temperature T_1. It can be seen that this series of numbers becomes more negative with increasing time; that is, the absolute value of the difference between $I_{K,n}$ and $I_{K,b}$ is increasing as n is increasing. The general expression for these difference peak areas, ΔI_K, can be obtained by substitution of eq A5 for $I_{K,n}$ with $I_{K,initial}$ set equal to $I_{K,1}$ for the first data point recorded at $t = 0$. Thus,

$$\Delta I_K = I_{K,n} - I_{k,b}$$
$$= \frac{I_{K,1} - I_{K,final}}{1 + k'tI_{K,1}} + (I_{K,final} - I_{K,b}) \qquad (A7)$$

for $0 < t < t_n$. Multiplying both sides of eq A7 by -1 leads to the increasing positive valued concave down function for $0 < t < t_n$ given by eq A8:

$$-\Delta I_K = I_{K,b} - I_{K,n}$$
$$= (I_{K,b} - I_{K,final}) - \frac{I_{K,1} - I_{K,final}}{1 + k'tI_{K,1}} \qquad (A8)$$

The recorded ketene kinetic trace for the *absolute value* of the difference peak area, $-\Delta I_K$, as a function of time appears as a *growth* and is consistent with the formalism of eq A8. Such a growth represents the increasing consumption of ketene during the progress of the reaction. In the case of the absorption peak due to the zwitterion, a similar analysis using eq A6 also results in a growth trace for the absolute value of the difference peak intensity, ΔI_Z, as a function of time, which would be consistent with our intuitive expectations for the appearance of the reaction product; namely,

$$\Delta I_Z = \frac{k''tI_{Z,1}(I_{Z,final} - I_{Z,1})}{1 + k''tI_{Z,1}} + (I_{Z,1} - I_{Z,b}) \qquad (A9)$$

for $0 < t < t_n$, where $I_{Z,initial}$ is set equal to $I_{Z,1}$ for the first data point recorded at $t = 0$. Equation A9 is an increasing positive valued concave down function with $\Delta I_Z = I_{Z,n} - I_{Z,b} > 0$ representing the increasing production of the zwitterion during the reaction.

Appendix B

Derivation of Hamill's Time-Dependent Activation Energy Expression.[28] From the time-dependent rate constant expression $k(t) = \alpha k_0{}^\alpha t^{\alpha-1}$, the time dependence of the activation is obtained as shown below:

$$k(t) = \alpha k_0(k_0 t)^{\alpha-1}$$
$$= \alpha k_0(t/\tau_0)^{\alpha-1}, \quad \text{since } k_0 = 1/c^{1/\alpha}\tau_0$$
$$= \alpha k_0 \exp[\ln(t/\tau_0)^{\alpha-1}]$$
$$= \alpha A_0 \exp\left[-\frac{E_0}{RT}\right] \exp[\ln(t/\tau_0)^{\alpha-1}], \quad \text{since } k_0 = A_0 \exp\left[-\frac{E_0}{RT}\right]$$
$$= \alpha A_0 \exp\left[-\frac{E_0 + (1-\alpha)RT\ln(t/\tau_0)}{RT}\right]$$

where E_0 is the average activation energy. Hence,

$$E(t) = E_0 + (1 - \alpha)RT\ln(t/\tau_0) \qquad (B1)$$

Appendix C

Probability Density Function. The density function in eq 13 satisfies the property

$$\int_{-\infty}^{\infty} f(z)\,dz = 1 \qquad (C1)$$

Hence,

$$\int_{-\infty}^{\infty} \frac{\sin(\pi\alpha)}{\pi} \frac{\exp(z\alpha)}{\exp(2z\alpha) + 2\exp(z\alpha)\cos(\pi\alpha) + 1}\,dz$$
$$= \frac{\sin(\pi\alpha)}{\pi} \int_{-\infty}^{\infty} \frac{\exp(z\alpha)}{\exp(2z\alpha) + 2\exp(z\alpha)\cos(\pi\alpha) + 1}\,dz$$
$$= \frac{\sin(\pi\alpha)}{\pi} \frac{1}{\alpha(B-A)}\left[\ln\left(\frac{\exp(z\alpha) + A}{\exp(z\alpha) + B}\right)\right]\Bigg|_{-\infty}^{\infty}$$
$$= \frac{\sin(\pi\alpha)}{\pi\alpha} \frac{\ln\left(\frac{B}{A}\right)}{B - A}$$
$$= \frac{\sin(\pi\alpha)}{\pi\alpha} \frac{\pm 2i\pi\alpha}{\pm 2i\sin(\pi\alpha)}$$
$$= 1$$

Note that $A = \exp(\pm i\pi\alpha)$ and $B = \exp(\mp i\pi\alpha)$.

Mean and Variance. From the density function given in eq 13, the average value of z is then

$$\langle z\rangle = \langle\ln(\tau/\tau_0)\rangle$$
$$= \int_{-\infty}^{\infty} zf(z)\,dz \qquad (C2)$$
$$= \frac{\sin(\pi\alpha)}{\pi} \int_{-\infty}^{\infty} \frac{z\exp(z\alpha)}{\exp(2z\alpha) + 2\cos(\pi\alpha)\exp(z\alpha) + 1}\,dz$$

Since $zf(z)$ is an odd function, then the definite integral is equal to zero and

$$\langle z\rangle = \langle\ln(\tau/\tau_0)\rangle = 0 \qquad (C3)$$

The variance, $\sigma_z{}^2$, is given by

$$\sigma_z{}^2 = \langle z^2\rangle - \langle z\rangle^2 \qquad (C4)$$

Again, from eq 13,

$$\langle z^2\rangle = \int_{-\infty}^{\infty} z^2 f(z)\,dz$$

$$= \frac{\sin(\pi\alpha)}{\pi}\int_{-\infty}^{\infty}\frac{z^2\exp(z\alpha)}{\exp(2z\alpha)+2\exp(z\alpha)\cos(\pi\alpha)+1}\,dz$$

$$= \frac{\sin(\pi\alpha)}{\pi}\,2\int_{-\infty}^{\infty}\frac{z^2\exp(z\alpha)}{\exp(2z\alpha)+2\exp(z\alpha)\cos(\pi\alpha)+1}\,dz,$$

since $z^2 f(z)$ is an even function

$$= \frac{\sin(\pi\alpha)}{\pi}\,2\,\frac{\pi^3}{6}\left(\frac{1-\alpha^2}{\alpha^2}\right)\frac{1}{\sin(\pi\alpha)}$$

$$= \frac{\pi^2}{3}\left(\frac{1-\alpha^2}{\alpha^2}\right) \qquad \text{(C5)}$$

where the relation[29] was used to evaluate the definite integral

$$\int_0^{\infty}\frac{x^2\,dx}{e^x+e^{-x}+2\cos\lambda} = \frac{1}{6}\lambda(\csc\lambda)(\pi^2-\lambda^2) \qquad \text{(C6)}$$

Substitution of eqs C3 and C5 in eq C4 yields

$$\sigma_z^{\,2} = \frac{\pi^2}{3}\left(\frac{1-\alpha^2}{\alpha^2}\right) \qquad \text{(C7)}$$

Derivation of k_0 as Geometric Mean of Rate Constants. Rewriting eq C3 in terms of rate constants we have $\langle\ln(k_0/k)\rangle = 0$. If the rate constants are treated as discrete random variables, then

$$\langle\ln(k_0/k)\rangle = \langle\ln k_0 - \ln k\rangle$$

$$= \frac{1}{N}\sum_j[\ln k_0 - \ln k_j] \qquad \text{(C8)}$$

$$= \ln k_0 - \frac{1}{N}\sum_j \ln k_j$$

From $\langle\ln(k_0/k)\rangle = 0$,

$$N\ln k_0 = \sum_j \ln k_j$$

$$\exp(N\ln k_0) = \exp(\ln k_1 + \ln k_2 + \ldots + \ln k_N)$$

$$k_0^{\,N} = k_1 k_2 \ldots k_N$$

and hence,

$$k_0 = \left[\prod_j k_j\right]^{1/N} \qquad \text{(C9)}$$

References and Notes

(1) (a) Platz, M. S.; Senthilnathan, V. P.; Wright, B. B.; McCurdy, C. W. *J. Am. Chem. Soc.* **1982**, *104*, 6494. (b) Senthilnathan, V. P.; Platz, M. S. *J. Am. Chem. Soc.* **1980**, *102*, 7637. (c) Lin, C. T.; Gaspar, P. P. *Tetrahedron Lett.* **1980**, *21*, 3553. (d) Platz, M. S. *Acc. Chem. Res.* **1988**, *21*, 236.

(2) (a) McMahon, R. J.; Chapman, O. L. *J. Am. Chem. Soc.* **1987**, *109*, 683. (b) Wierlacher, S.; Sander, W.; Liu, M. T. H. *J. Am. Chem. Soc.* **1993**, *115*, 8943.

(3) Ambroz, H. B.; Kemp, T. J. *J. Chem. Soc., Faraday Trans. 1* **1982**, *78*, 725.

(4) Sprague, E. D. *J. Phys. Chem.* **1977**, *81*, 516.

(5) Buchwalter, S. L.; Closs, G. L. *J. Am. Chem. Soc.* **1979**, *101*, 4688.

(6) Sponsler, M. B.; Jain, R.; Coms, F. D.; Dougherty, D. A. *J. Am. Chem. Soc.* **1989**, *111*, 2240.

(7) Kohlrausch, F. *Pogg. Ann.* **1863**, *119*, 337.

(8) (a) Plonka, A. *Annu. Rep. Prog. Chem., Sect. C* **1989**, *85*, 47 and references therein. (b) Eberlein, J.; Creuzburg, M. J. *Chem. Phys.* **1997**, *106*, 2188. (c) Marcinek, A.; Gebicki, J.; Plonka, A. *J. Phys. Org. Chem.* **1990**, *3*, 757. (d) Gebicki, J.; Plonka, A.; Krantz, A. *J. Chem. Soc., Perkin Trans. 2* **1990**, 2051. (e) Plonka, A. *Chem. Phys. Lett.* **1988**, *151*, 466.

(9) (a) Stepanov, A. A.; Tkatchenko, V. A.; Bol'shakov, B. V.; Tolkatchev, T. A. *Int. J. Chem. Kinet.* **1978**, *10*, 637. (b) Bol'shakov, B. V.; Stepanov, A. A.; Tolkatchev, V. A. *Int. J. Chem. Kinet.* **1980**, *12*, 271. (c) Bol'shakov, B. V.; Tolkatchev, T. A. *Chem. Phys. Lett.* **1976**, *40*, 468.

(10) (a) Plonka, A. In *Lecture Notes in Chemistry No. 40*; Berthier, M., Dewar, M. J. S., Fischer, H., Fukui, K., Hall, G. G., Hartmann, H., Jaffe, H. H., Jortner, J., Kutzelnigg, W., Ruedenberg, K., Tomasi, J., Eds.; Springer-Verlag: Berlin, 1986; Chapter 6. (b) Scher, H.; Montroll, E. W. *Phys. Rev. B* **1975**, *12*, 2455. (c) Hamill, W. H.; Funabashi, K. *Phys. Rev. B* **1977**, *16*, 5523.

(11) (a) Plonka, A.; Paszkiewicz, A. *Chem. Phys.* **1996**, *212*, 1. (b) Plonka, A. *Radiat. Phys. Chem.* **1991**, *37*, 411. (c) Plonka, A. *Radiat. Phys. Chem.* **1986**, *28*, 429. (c) Plonka, A.; Berlin, Y. A.; Chekunaev, N. I. *Chem. Phys. Lett.* **1989**, *158*, 380.

(12) (a) Plonka, A. *J. Polym. Sci., Polym. Phys. Ed.* **1983**, *21*, 1011. (b) Patel, V. M.; Patel, G. N.; Gvozdic, N.; Hsu, C. S.; Dole, M. *J. Polym. Sci., Polym. Phys. Ed.* **1978**, *16*, 467. (c) Szöcs, F.; Placek, J.; Kotlarik, B. *J. Appl. Polym. Sci.* **1977**, *21*, 859. (d) Plonka, A. *Radiat. Phys. Chem.* **1991**, *37*, 555.

(13) (a) Plonka, A. *Radiat. Phys. Chem.* **1983**, *21*, 405. (b) Szajdzinska-Pietek, E.; Kroh, J.; Plonka, A. *Radiat. Phys. Chem.* **1982**, *20*, 135. (c) Roy, C. R.; Willard, J. E. *J. Phys. Chem.* **1972**, *76*, 1405.

(14) Plonka, A. *Radiat. Phys. Chem.* **1987**, *30*, 31.

(15) Plonka, A.; Kroh, J.; Berlin, Y. A. *Chem. Phys. Lett.* **1988**, *153*, 433. An abbreviated proof of eq 10 containing errors appears in this reference. See the Supporting Information for an expanded and corrected proof.

(16) Plonka, A.; Lefik, W.; Kroh, J. *Radiat. Phys. Chem.* **1990**, *36*, 191.

(17) (a) Andraos, J.; Kresge, A. J. *J. Am. Chem. Soc.* **1992**, *114*, 5643. (b) Allen, A. D.; Tidwell, T. T. *J. Org. Chem.* **1999**, *64*, 266. (c) Barra, M.; Fisher, T. A.; Cenigliaro, G. J.; Sinta, R.; Scaiano, J. C. *J. Am. Chem. Soc.* **1992**, *114*, 2630. (d) Wang, J. L.; Toscano, J. P.; Platz, M. S.; Nikolaev, V.; Popik, V. V. *J. Am. Chem. Soc.* **1995**, *117*, 5477. (e) Wagner, B. D.; Arnold, B. R.; Brown, G. S.; Lusztyk, J. *J. Am. Chem. Soc.* **1998**, *120*, 1827. (f) Oishi, S.; Ozaki, J. *Chem. Lett.* **1998**, 1071. (g) Visser, P.; Zuhse, R.; Wong, M. W.; Wentrup, C. *J. Am. Chem. Soc.* **1996**, *118*, 12598.

(18) (a) Sung, K.; Tidwell, T. T. *J. Am. Chem. Soc.* **1998**, *120*, 3043. (b) D.-C. Fang; Fu, X.-Y. *J. Mol. Struct. (THEOCHEM)* **1998**, *455*, 59.

(19) Qiao, G. G. H.; Andraos, J.; Wentrup, C. *J. Am. Chem. Soc.* **1996**, *118*, 5634. The term "ketene ylide" is a misnomer and is discouraged as the structures of the zwitterionic adducts do not fit the formal definition of an ylide structure as noted in the following: Muller, P. *Pure Appl. Chem.* **1994**, *66*, 1077.

(20) (a) Andraos, J.; Chiang, Y.; Kresge, A. J.; Popik, V. V. *J. Am. Chem. Soc.* **1997**, *119*, 8417. (b) Andraos, J.; Chiang, Y.; Huang, C. H.; Kresge, A. J.; Scaiano, J. C. *J. Am. Chem. Soc.* **1993**, *115*, 10605. (c) Urwyler, B.; Wirz, J. *Angew. Chem., Int. Ed. Engl.* **1990**, *29*, 790. (d) Almstead, J. K.; Urwyler, B.; Wirz, J. *J. Am. Chem. Soc.* **1994**, *116*, 954. (e) Andraos, J. Ph.D. Thesis, University of Toronto, 1991.

(21) (a) deLucas, N. C.; Netto-Ferreira, J. C.; Andraos, J.; Lusztyk, J.; Wagner, B. D.; Scaiano, J. C. *Tetrahedron Lett.* **1997**, *38*, 5147. (b) Andraos, J.; deLucas, N. C.; Scaiano, J. C. Unpublished results.

(22) For an absorption band that is described by a Gaussian function we have $A(\omega) = A_0\exp[-(\omega-\omega_0)^2/\sigma^2]$ where A_0 is the maximum amplitude, ω_0 is the wavenumber value at maximum absorbance, and σ is the width parameter. The peak height is then A_0 and the peak area, I, found by integration of $A(\omega)$ over the range $\omega \in (-\infty,+\infty)$ is equal to $A_0\sigma\sqrt{\pi}$.

(23) (a) Raff, L. M. In *Multidimensional Molecular Dynamics Methods*; Thompson, D. L., Ed.; World Scientific Publishers: London, 1997. (b) Spath, B. W.; Raff, L. M. *J. Phys. Chem.* **1992**, *96*, 2179.

(24) Mendenhall, W.; Wackerly, D. D.; Scheaffer, R. L. *Mathematical Statistics with Applications*, 4th ed.; PWS−Kent Publishing Co.: Boston, 1990.

(25) (a) Rhodes, T. A.; Fox, M. A. *J. Phys. Chem.* **1996**, *100*, 17931. (b) Siemiarczuk, A.; Ware, W. R. *Chem. Phys. Lett.* **1987**, *140*, 277. (c) Siemiarczuk, A.; Ware, W. R. *J. Phys. Chem.* **1987**, *91*, 3677. (d) James, D. R.; Liu, Y. S.; De Mayo, P.; Ware, W. R. *Chem. Phys. Lett.* **1985**, *120*, 460. (e) James, D. R.; Ware, W. R. *Chem. Phys. Lett.* **1985**, *120*, 455. (f) James, D. R.; Ware, W. R. *Chem. Phys. Lett.* **1986**, *126*, 7.

(26) (a) Cvetanovic, R. J.; Singleton, D. L.; Paraskevopoulos, G. *J. Phys. Chem.* **1979**, *83*, 50. (b) Cvetanovic, R. J.; Singleton, D. L. *Int. J. Chem. Kinet.* **1977**, *9*, 481. (c) Cvetanovic, R. J.; Singleton, D. L. *Int. J. Chem. Kinet.* **1977**, *9*, 1007. (d) Heberger, K.; Kemeny, S.; Vidoczy, T. *Int. J. Chem. Kinet.* **1987**, *19*, 171. (e) Kalantar, A. H. *Chem. Eng. J.* **1987**, *34*, 159.

(27) (a) Bothe, E.; Dessouki, A. M.; Schulte-Frohlinde, D. *J. Phys. Chem.* **1980**, *84*, 3270. (b) Allen, B. M.; Hegarty, A. F.; O'Neill, P.; Nguyen, M. T. *J. Chem. Soc. Perkin Trans. 2* **1992**, 927. (c) Jähme, J.; Rüchardt, C. *Tetrahedron Lett.* **1982**, *23*, 4011.

(28) Hamill, W. H. *Chem. Phys. Lett.* **1981**, *77*, 467.

(29) (a) de Haan, D. B. *Nouvelles Tables D'Intégrales Définies*; G. E. Stechert & Co.: New York, 1939. (b) Gradshteyn, I. S.; Ryzhik, I. M. *Table of Integrals, Series, and Products*, 5th ed.; Academic Press: Boston, 1994.